electronics

MDPI

Article

Neural Network Based Robust Lateral Control for an Autonomous Vehicle

Subrat Kumar Swain [1], Jagat J. Rath [2] and Kalyana C. Veluvolu [3,*]

[1] Graduate School of Electronics and Electrical Engineering, Kyungpook National University, Daegu 41566, Korea; skswain@knu.ac.kr
[2] Department of Mechanical and Aero-Space Engineering, Institute of Infrastructure Technology Research and Management, Gujarat 380026, India; jagatjyoti.rath@gmail.com
[3] School of Electronics Engineering, Kyungpook National University, Daegu 41566, Korea
* Correspondence: veluvolu@ee.knu.ac.kr

Abstract: The lateral motion of an Automated Vehicle (AV) is highly affected by the model's uncertainties and unknown external disturbances during its navigation in adverse environmental conditions. Among the variety of controllers, the sliding mode controller (SMC), known for its robustness towards disturbances, is considered to generate a robust control signal under uncertainties. However, conventional SMC suffers from the issue of high frequency oscillations, called chattering. To address the issue of chattering and reduce the effect of unknown external disturbances in the absence of precise model information, a radial basis function neural network (RBFNN) is employed to estimate the equivalent control. Further, a higher order sliding mode (HOSM) based switching control is proposed in this paper to compensate for the effect of external disturbances. The effectiveness of the proposed controller in terms of lane-keeping and lateral stability is demonstrated through simulation in a high-fidelity Carsim-Matlab Simulink environment under a variety of road and environmental conditions.

Keywords: Automated Vehicle; higher order sliding mode; radial basis function neural network; lane-keeping; lateral stability

Citation: Swain, S.K.; Rath, J.J.; Veluvolu, K.C. Neural Network Based Robust Lateral Control for an Autonomous Vehicle. *Electronics* **2021**, *10*, 510. https://doi.org/10.3390/electronics10040510

Academic Editor: Arturo de la Escalera Hueso

Received: 26 January 2021
Accepted: 16 February 2021
Published: 22 February 2021

1. Introduction

The technological progress in the field of transportation has called for the need of a safe and hassle free driving experience in the presence of diverse, challenging environments. Driverless cars have proved to be a remarkable step towards automation, marking a paradigm shift from the manual driving (MD) scenario. MD is often prone to human-centric errors occurring due to the carelessness and inattentiveness of the driver leading to a risk for the individual and traffic safety [1]. Automated vehicles (AV) on the other hand, equipped with state-of-the-art sensors, are expected to reduce the driver burden along with ensuring driver comfort and vehicle safety [2–4]. AV have shown promising progress in path planning [5], path tracking [6–8] and decision making fields [9] that are crucial for autonomous driving.

Lateral and longitudinal control are the two major areas regulating the overall motion of AV. Lane-keeping and lateral stability are the two primary objectives for the lateral control whereas the velocity control is the primary aspect for the longitudinal control of the vehicle. For the lane-keeping purpose, the path following controllers designed using PID [10], sliding mode [8,11] and Model Predictive Control (MPC) [7,12,13] have been discussed in the literature. In order to address the path tracking objective involving complex maneuvers, the design of a PID controller employing various design approaches to adjust the controller parameters was discussed in [14]. The lateral control of autonomous vehicles in the event of unknown road curvature using a nested PID steering control was proposed in [10]. However, the above studies did not take into account the impact of

aerodynamic forces on the vehicular lateral control. PID control, which is considered one of the simplest and easily constructed controllers for lane-keeping, suffers from the performance issues when there is a change in the external environment. A nonlinear model predictive control (NMPC) approach for the purpose of yaw motion control by utilizing the C/GMRES algorithm for distributed drive electric vehicles was proposed in [15]. The key idea behind applying the C/GMRES algorithm was to address the computational cost of NMPC for distributed drive electric vehicles. The issue of path following control by considering the vehicle constraints such as yaw-rate, steering angle, lateral position error and side-slip angle was addressed in [16]. However, the aforementioned papers [15,16] did not consider the effect of external disturbances such as crosswinds and yaw-moment on the lateral motion of the vehicle. The simultaneous control of lateral and longitudinal motion of the vehicle by employing a neural network based adaptive controller was suggested in [17]. The purpose of designing the proposed controller was to achieve the path following and speed tracking control requirements. However, this paper did not consider the adverse environmental conditions such as vehicles moving on low friction surfaces in the presence of crosswinds. An LMI based TS Fuzzy static output feedback control scheme for the path following of autonomous vehicles was proposed in [18]. The vehicle was subjected to the road curvature disturbances and time-varying vehicle speed scenarios. However, the combined road vehicle control model neglected the impact of aerodynamic forces on the lateral motion of the vehicle under adverse road conditions. A comparative study evaluating the performance of an unmanned surface vehicle (USV) in terms of station keeping heading and position using a nonlinear proportional derivative, sliding mode, and backstepping feedback controllers in the presence of wind disturbances was proposed in [19]. However, the type of autonomous vehicles taken into consideration in this paper was marine vehicles.

Sliding mode control (SMC) has an inherent ability to compensate for matched uncertainties and unknown disturbances. However, the conventional first order SMC exhibit high frequency chattering in its control action, which is quite undesirable. To address the issue of chattering in the SMC, several approaches based on non-singular terminal SMC (NT-SMC) [20] and higher order sliding mode (HOSM) [21] have been proposed. NT-SMC and HOSM approaches can effectively suppress the chattering phenomenon and simultaneously compensate for the effect of disturbances in finite time. However, the control based approaches discussed in the literature are effective in implementation as long as the perfect knowledge of the system is in place. On the contrary, in the realistic scenario, the information regarding the model dynamics is limited. The model uncertainties and the disturbances are time-varying and they are dependent on the change in the navigational environment. In those cases, it becomes difficult to measure those entities and thus the design of model based control approaches fail to achieve the objective.

To address the shortcomings in the model based control approaches discussed above, model free based control approaches have been proposed for ensuring lane-keeping (LK) and lateral stability (LS) of the vehicle [22–24]. The authors in [22] proposed an adaptive neural network (ANN) approximator to estimate the uncertainty in the tire cornering coefficient and laid down the design of a backstepping variable structure control (BSVC) to compensate the lateral deviation and oscillations in the yaw-rate of the vehicle. This paper takes into consideration the vehicle maneuvering in the low-friction surfaces where the proposed neural network based controller was able to compensate for the undesirable yaw-moment generating oscillations in the yaw-rate. However, the authors in [22] do not take into consideration the effect of crosswinds and yaw-moment as external disturbances affecting the lateral motion of the vehicle. In [23], the authors proposed a hybrid combination of a fuzzy neural network and SMC to develop a lateral control strategy to track a desired trajectory. However, the issue associated with the fuzzy control approach is the choice of rules in designing the control law. In the fuzzy control approach, the choice of rules highly impact the control performance of the system. Incorrect choice of rules does not provide an optimal control performance leading to either sub-optimal or deteriorated

performance. Again the choice of rules highly depends on an accurate or near to accurate knowledge of the system, which is not available every time. In addition, the choice of membership function is also arbitrary and therefore to get an efficient control performance in the fuzzy control approach is a challenging aspect.

Motivated by the idea of robust lateral control of the vehicle presented in [22], this paper takes into consideration the effect of crosswinds and yaw-moment as external disturbances affecting the lateral motion of the vehicle. The type of autonomous vehicles taken into consideration in this paper are the car-like vehicles with an Ackermann geometry model. The vehicle traversing with Ackermann steering states that the outer wheel steers for a smaller angle than the inner wheel. The front left wheel serves as the outer wheel whereas the front right wheel acts as the inner wheel. In the current study, which is based on the path tracking objective, the vehicle model taken into consideration is the vehicle dynamics based dynamic bicycle model equipped for higher vehicle speeds. The reason behind not considering the kinematic bicycle model is because at higher speeds the velocity at each wheel is not in the direction of the wheel. The main contributions related to this research work are as follows:

- The tire cornering stiffness exhibits strong uncertainty under challenging driving conditions in the presence of unknown external disturbances. To deal with such types of conditions, this paper proposes a HOSMC based radial basis function neural network (RBFNN) to maintain lateral control and yaw stability of the vehicle.
- An overall closed-loop stability of the HOSMC based RBFNN for the bicycle model of the vehicle is established. The weights of the neural network are adjusted online with the formulation of an adaptation law using the Lyapunov method thereby ensuring convergence of the sliding surface error.
- Simulations are performed in the CarSim-Matlab Simulink environment to justify the performance of the proposed neural network based controller.

This paper is organized as follows. Section 2 presents a brief description regarding the governing dynamics affecting the lateral dynamics of the vehicle. Section 3 provides an overview of the robust HOSM controller design whereas Section 4 lays down the detailed procedure regarding the proposed RBFNN based HOSMC design for compensating the effect of uncertainties and disturbances affecting the lateral motion of the vehicle. This section also discusses the overall closed loop stability exhibited by the proposed controller. Section 5 discusses the simulation results showing the robust performance of the vehicle with respect to the LK and LS as performance indices. Section 6 provides a brief discussion on the simulation results, whereas Section 7 concludes the paper.

2. Vehicle Dynamic Model

The lateral vehicle dynamics model is expressed as [25,26].

$$\begin{aligned} mv_x\dot{\beta} &= F_f + F_r - mv_x n + F_y \\ I_z\dot{n} &= l_f F_f - l_r F_r + M_z \end{aligned} \tag{1}$$

where $m, v_x, I_z, \beta, n, F_f, F_r$ represent the mass of the vehicle, longitudinal velocity, yaw inertia, side-slip angle, yaw-rate, front and rear friction forces acting on the vehicle. l_f, l_r represent the distance of the front wheel and rear wheel from the center of gravity. F_y and M_z represent the lateral forces applied on the vehicle due to the effect of crosswinds and the yaw-moment, respectively. The crosswinds and the yaw-moment represent the unknown external disturbances. As far as crosswinds are concerned, a strong gust of wind generates sufficient force and torque that can roll over or drive the vehicle out of the lane. More specifically, the effect of crosswinds on the lateral offset and stability of the vehicle is pronounced when the vehicle is moving at a higher longitudinal speed on low-friction surfaces. The resulting aerodynamic forces and the moment that act on the vehicles rigid body are represented in longitudinal, lateral and vertical directions. Since this study is focused on the lateral control of the AV, the aerodynamic forces on the lateral direction is

represented as $F_w = \frac{1}{2}\rho C_F A v_{rel}^2$ and $M_z = \frac{1}{2}\rho C_M A L v_{rel}^2$ where ρ, A, L and v_{rel} represent the air density, vehicle area, vehicle length and relative wind speed, respectively. C_F and C_M represent the non-dimensional coefficients corresponding to the force and moment, respectively. Generally, the crosswinds impact the vehicle at various incident angles and for this study, we have assumed the wind's impact at an incident angle of 75 degrees. For the vehicle to satisfy the lane-keeping task, the objective is to keep the vehicle near to the center lane with minimum lateral offset and orientation error. In addition to the lane-keeping task, the other objective is to ensure stability of the vehicle by minimizing the oscillations in the yaw-rate during high lateral accelerations or low frictional surfaces. In order to satisfy the above objectives, the lane dynamics with road curvature ρ should include the lateral offset y_{ld} and heading error ϕ_{ld} term at look ahead distance l_d. Thus the dynamics of the lane tracking error is expressed as [25]

$$\begin{aligned} \dot{y}_{ld} &= v_y + l_d n + \phi_{ld} v_x \\ \dot{\phi_{ld}} &= n - \rho v_x \end{aligned} \tag{2}$$

Considering the linear relationship between the tire lateral forces and the slip angle, the expression for the front and the rear axle lateral forces can be represented as

$$\begin{aligned} F_f &= \mu C_f \alpha_f \\ F_r &= \mu C_r \alpha_r \end{aligned} \tag{3}$$

where C_f, C_r represent the tire cornering coefficients. α_f, and α_r represent the front and rear tire slip angles, which is expressed as

$$\begin{aligned} \alpha_f &= \delta_f - \beta - \frac{l_f n}{v_x} \\ \alpha_r &= -\beta + \frac{l_r n}{v_x} \end{aligned} \tag{4}$$

where δ_f represent the front wheel road steer angle. Figure 1 shows the combined vehicle dynamics with the lane tracking errors considered in this study.

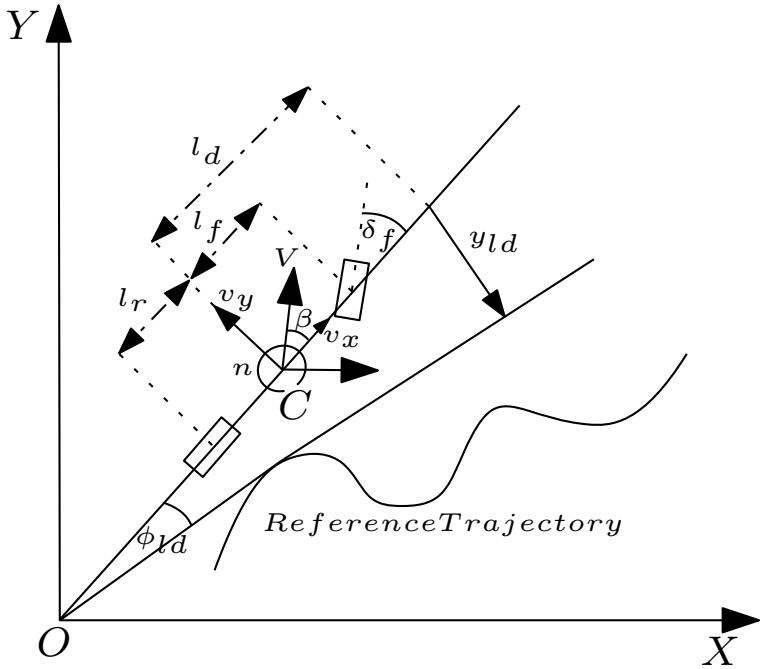

Figure 1. Combined vehicle dynamics and the kinematic model.

3. Robust HOSMC Design

Figure 2 shows the overall architecture of the proposed neural network based controller for the lateral control of the vehicle.

In Figure 2 the sliding surface ρ is a function of lateral error e, which acts as the input to the proposed RBFNN based HOSM controller. On the account of unknown external disturbances affecting the system, the proposed RBFNN is used to estimate the equivalent control input $\hat{\delta}_{eq}$. The robust term v computed from the HOSM configuration along with the estimated equivalent control input generates the optimal road steer angle δ_f, which acts as the control input for the vehicle model. The desired lateral offset y_{ref}, which is taken as the reference should be zero at look ahead distance l_d. Thus the sliding surface σ is designed as

$$e = y_{ref} - y_{ld} = -y_{ld} \tag{5}$$

$$\sigma = \dot{e} + \lambda e = v_y + l_d n + \phi_{ld} v_x + \lambda y_{ld} \tag{6}$$

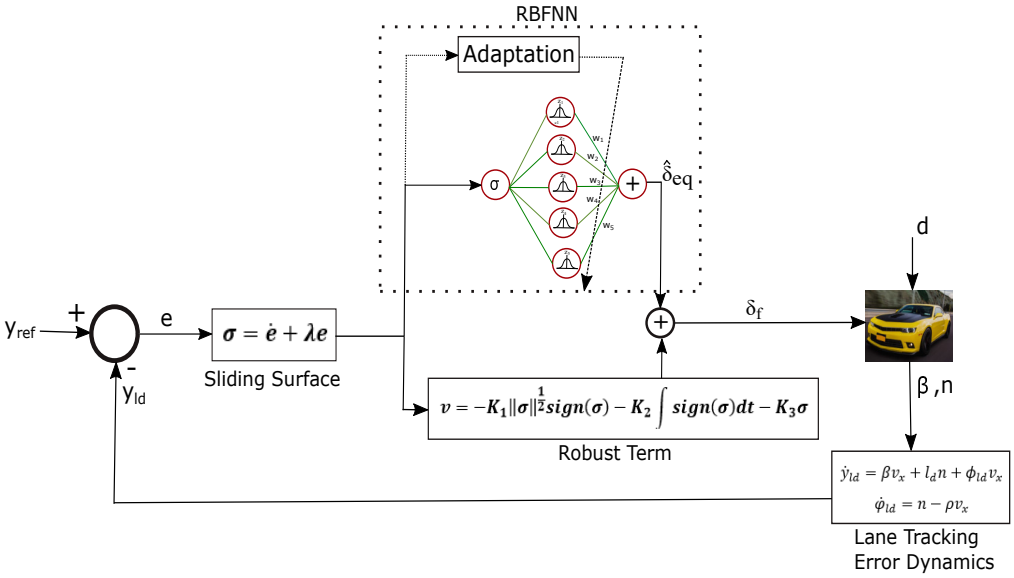

Figure 2. Overall schematic of the closed-loop radial basis function neural network (RBFNN) based higher order sliding mode controller (HOSMC) for the lateral control of the vehicle. y_{ld}: lateral offset at look ahead distance l_d, ϕ_{ld}: heading error at look ahead distance l_d, n: yaw-rate, β: side-slip angle, δ_f: road steer angle, d: unknown disturbances acting on the front wheel angle, y_{lr}: reference projected error.

In the case of adverse conditions such as at the low friction surface or high lateral acceleration, the tire cornering characteristics exhibit high uncertainty. The tire cornering coefficients can then be expressed as $C_f = C_{fn} + f_{cf}(.)$ and $C_r = C_{rn} + f_{cr}(.)$ where, C_{fn} and C_{rn} represent the nominal values of tire cornering coefficients. $f_{cf}(.)$ and $f_{cr}(.)$ represent the uncertainty in the tire cornering characteristics. Thus from Equations (1)–(4), the derivative of the sliding surface is expressed as

$$\dot{\sigma} = \ddot{e} + \lambda\dot{e} = f + \lambda(v_y + l_d n + \phi_{ld} v_x) + g\delta_f + d \tag{7}$$

where $f = \frac{\mu}{m}(C_{fn}(-\beta - \frac{l_f n}{v_x}) + C_{rn}(-\beta - \frac{l_r n}{v_x})) + \frac{\mu l_d}{I_z}(l_f C_{fn}(-\beta - \frac{l_f n}{v_x}) - l_r C_{rn}(-\beta + \frac{l_r n}{v_x})) - \rho v_x^2 + \zeta(.)$, $\zeta(.) = \frac{\mu}{m}(f_{cf}(.)\alpha_f + f_{cr}(.)\alpha_r) + \frac{\mu l_d}{I_z}(l_f f_{cf}\alpha_f - l_r f_{cr}\alpha_r)$, $g = \frac{\mu C_{fn}}{m} + \frac{\mu l_d l_f C_{fn}}{I_z}$ and $d = \frac{F_y}{m} + \frac{l_d M_z}{I_z}$.

From (7), it is observed that the term f contains the tire-force uncertainty $\zeta(.)$ and d represents the effect of crosswinds and yaw-moment on the lateral motion of the vehicle. λ

represents the design parameter satisfying $\lambda > 0$. For the existence of second order sliding control, $\dot{\sigma} = 0$ should be satisfied. Thus, for the convergence of the sliding error in the presence of disturbances, the front wheel steering angle is then expressed as

$$\delta_f = \delta_{eq} + \delta_{rob} = \frac{1}{g}(-f - \lambda(v_y + l_d n + \phi_{ld} v_x) + v) \tag{8}$$

where δ_{eq} and δ_{rob} represent the equivalent road steer angle and the robust control term, respectively. v represents the robust term, which is expressed as [27]

$$v = -k_1 \|\sigma\|^{\frac{1}{2}} sign(\sigma) - k_2 \int sign(\sigma) dt - k_3 \sigma \tag{9}$$

Here, k_1, k_2, k_3 represent the positive robust term gains to be designed accordingly. For this study, the gains associated with the HOSM controller are $k_1 = 0.005$, $k_2 = 0.00002$, and $k_3 = 0.008$, respectively. The higher the longitudinal speed, the higher the tire cornering force. The value of tire-force uncertainty $\zeta(.)$, which is difficult to estimate, also changes with the change in the longitudinal speed and the road surface conditions. Thus, the term f in (8) that regulates the equivalent road steer angle δ_{eq} is also difficult to estimate as it consists of the tire-force uncertainty term. The dynamics of crosswinds and the yaw-moment also depend on the longitudinal speed of the vehicle. The higher the speed, the greater the lateral force and yaw-moment impacted on the vehicle. To address the above challenges and its impact on the lateral control of the vehicle, an adaptive HOSMC based on RBFNN is proposed for effective lane-keeping and stability of the vehicle.

4. RBFNN Based HOSMC Design

The structure of RBFNN with one input and one output with a hidden layer consisting of five nodes is shown in Figure 3. The design procedure of the proposed controller includes the estimation of δ_{eq} using RBFNN. The input to this RBFNN structure is the sliding surface σ and the hidden layer consists of five nodes with a gaussian kernel, each one having a predefined center c and bias width b. The dynamics of RBFNN are expressed by

$$z_i(x) = e^{-\frac{\|x - c_i\|^2}{2b_i^2}} \tag{10}$$

where i ranges from 1 to 5. The center and the bias considered for this study is

$$c_i = \begin{bmatrix} -2 & -1 & 0 & 1 & 2 \end{bmatrix} \quad b_i = 0.75 \tag{11}$$

The ideal output δ_{eq} using the RBFNN dynamics from (10) is represented by

$$\delta_{eq} = \mathbf{W}^T z(x) + \triangle_f$$

where $\triangle_f$ represents a very small approximation error satisfying $\triangle_f \leq \triangle_f^+$ and $\mathbf{W}$ represents the weight vector. However, the approximated value of δ_{eq} using RBFNN is then represented by

$$\hat{\delta}_{eq} = \hat{\mathbf{W}}^T z(x)$$

where $\hat{\mathbf{W}}$ is the estimated value of $\mathbf{W}$ to be obtained. The approximate error in the equivalent road steer angle is then represented by

$$\tilde{\delta}_{eq} = \hat{\delta}_{eq} - \delta_{eq} = \tilde{\mathbf{W}}^T z(x) - \triangle_f \tag{12}$$

Now taking into consideration that $\delta_f = \hat{\delta}_{eq} + \delta_{dis}$ where $\hat{\delta}_{eq}$ and δ_{dis} represent the estimated equivalent value of the steering angle and the robust term, respectively. Referring to (7), (8) and (12) we get

$$\begin{aligned}\dot{\sigma} &= f + \lambda(v_y + l_d n + \phi_{ld} v_x) + g(\hat{\delta}_{eq} + \delta_{dis}) + d \\ &= f + \lambda(v_y + l_d n + \phi_{ld} v_x) + g(\tilde{\delta}_{eq} + \delta_{eq} + \delta_{dis}) + d \\ &= f + \lambda(v_y + l_d n + \phi_{ld} v_x) + g(\tilde{\delta}_{eq} + \frac{1}{g}(-f - \lambda(v_y + l_d n + \phi_{ld} v_x) + v)) + d \\ &= g\tilde{\delta}_{eq} + v + d \\ &= g(\tilde{\mathbf{W}}^T z(x) - \triangle_f) + v + d \end{aligned} \tag{13}$$

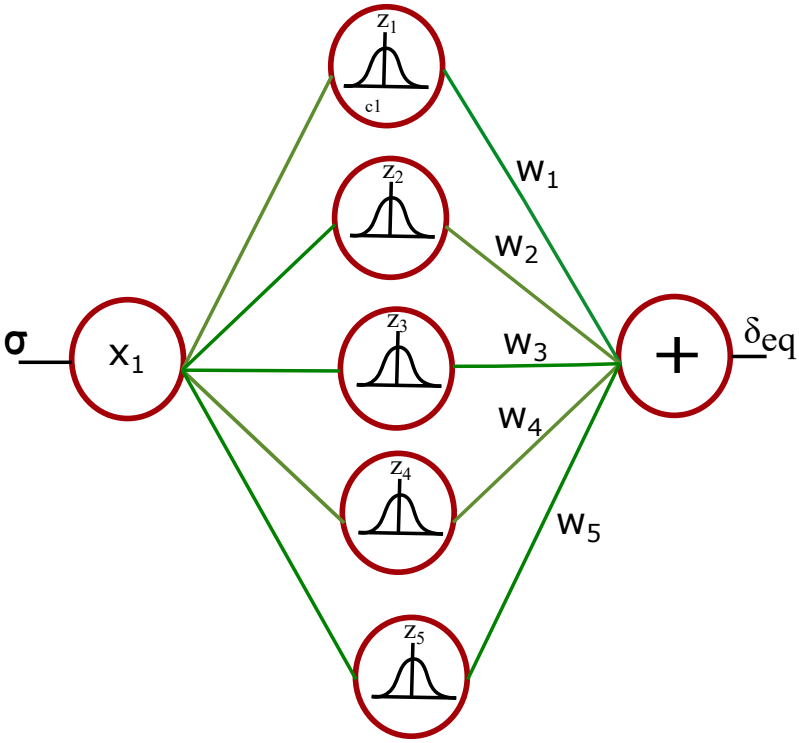

Figure 3. Structure of the RBFNN.

Closed-Loop Stability Analysis

In order to check for the stability of the proposed RBFNN based HOSMC, the Lyapunov candidate function selected is represented as

$$V = \frac{1}{2}\sigma^2 + \frac{1}{2\tau}\tilde{\mathbf{W}}^T\tilde{\mathbf{W}} \tag{14}$$

where τ represents the adaptive learning rate satisfying $\tau > 0$. The choice of τ greatly impacts the overall closed-loop performance in such a way that too small or too high a value of this parameter leads the system to the point of instability. Therefore the value of τ chosen for this study is 0.00005. The derivative of the $\tilde{\mathbf{W}}$ is represented as $\dot{\tilde{\mathbf{W}}} = \dot{\hat{\mathbf{W}}} - \dot{\mathbf{W}} = \dot{\hat{\mathbf{W}}}$ as $\mathbf{W}$ represents the ideal optimal weight and so its derivative $\dot{\mathbf{W}}$ will be zero. However, $\hat{\mathbf{W}}$ will get updated over the simulation interval till it reaches its optimal value. The derivative of the Lyapunov function V is then expressed as

$$\begin{aligned}\dot{V} &= \sigma\dot{\sigma} + \frac{1}{\tau}\tilde{\mathbf{W}}^T\dot{\tilde{\mathbf{W}}} \\ &= \sigma(g\tilde{\mathbf{W}}^T z(x) - g\triangle_f + v + d) + \frac{1}{\tau}\tilde{\mathbf{W}}^T\dot{\tilde{\mathbf{W}}} \\ &= \sigma(-g\triangle_f + v + d) + \tilde{\mathbf{W}}^T(\sigma g z(x) + \frac{1}{\tau}\dot{\tilde{\mathbf{W}}}) \end{aligned} \tag{15}$$

By ensuring $\dot{\tilde{\mathbf{W}}} = -\tau\sigma g z(x)$, Equation (15) becomes

$$\dot{V} = \sigma(-g\triangle_f + v + d) \tag{16}$$

From (16), it can be observed that if $\|v\| \geq max(-g\triangle_f + d)$, with $\|d\| < D$ where D represents the peak value of the disturbance, then the derivative of the Lyapunov function $\dot{V} < 0$ for $\sigma \neq 0$. As the control input δ_f from (8) is upper bounded such that $\delta_f \leq \delta_f^+$, so the RBF weight $\hat{\mathbf{W}}$ is ultimately bounded and the convergence of the $\hat{\mathbf{W}}$ to the optimal value is achieved.

5. Simulation Results

In this section, the performance of the vehicle in terms of lane-keeping errors (lane offset and heading error), and stability (yaw-rate and lateral acceleration) of the proposed scheme is evaluated and compared with the pure-pursuit MPC controller in the CarSim-Matlab Simulink environment. The Carsim vehicle simulator uses an in-built MPC for lateral control of the Automotive Vehicle. The objective of the controller is to ensure that the vehicle tracks a reference trajectory with minimum lateral error. The cost function associated with this MPC to be minimized is expressed as

$$\begin{aligned} \min_{u} \quad & J = \frac{1}{T}\int_0^T (z_{ref}(t) - z(t))^2 Q(t)\, dt \\ \text{s.t.} \quad & \dot{\mathbf{x}} = A\mathbf{x} + Bu + Lw \\ & z = C\mathbf{x} + Du + Nw \end{aligned}$$

where $\mathbf{x}$ represents the vehicle state, u represents the control input, which in our case is the road steer angle, w represents the disturbance affecting the system, and z represents the output of the system. The matrices A, B, C, D, L and N have constant coefficients. The control objective is to ensure that the control input u drives the vehicle in such a way that the output z tracks the given reference trajectory over a preview time T. The control input u is considered optimal when it minimizes the cost function J. The vehicle used in CarSim belongs to E-class Sedan and the tire model used in the study is the 225/60 R18 Internal tire model. The estimation of the equivalent control $\hat{\delta}_{eq}$ to compensate for the uncertainty and the effect of disturbances by the proposed controller is validated through simulation. The performance of the vehicle employing the proposed scheme is investigated with and without the effect of disturbances. Further, to validate the robustness of the proposed scheme, the vehicle is made to traverse on a variety of road conditions at various longitudinal velocities. The coefficient of friction μ for those road surfaces is varied from 0.4 to 1. The effectiveness of the proposed scheme is evaluated using a performance metric employing statistical measures such as Root Mean Square Error (RMSE) for lane-keeping errors and coefficient of variation (COV) for stability of the vehicle. The vehicle specifications considered for this study are shown in Table 1.

Table 1. Vehicle specifications.

Parameters	Description	Value
m	Vehicle mass	1653 kg
l_f	Front axle distance from the center of gravity	1.402 m
l_r	Rear axle distance from the center of gravity	1.646 m
C_{fn}	Tire cornering coefficient of front tire	390,550 $\frac{N}{rad}$
C_{rn}	Tire cornering coefficient of rear tire	571,680 $\frac{N}{rad}$
l_d	Look-ahead distance	7 m
I_z	Yaw-Inertia	2765 kg·m^2

5.1. Nominal Case: Vehicle Performance without the Impact of Disturbances

In this case, the performance of the vehicle in terms of lane-keeping errors and stability is studied when it is not impacted with any crosswinds. Here, the road friction coefficient (μ) is taken to be equal to 1. It is observed from Figures 4–6 that the proposed RBFNN-HOSM controller yields less lateral offset and renders better stability to the vehicle because of comparatively lesser peak magnitude of yaw-rate and lateral acceleration than compared to the pure pursuit in-built MPC controller in CarSim (CSM). The road steer angle of the proposed scheme, as shown in Figure 7, shows smooth response for the vehicle speedsv_x = 60 km/h and v_x = 100 km/h. It is evident from the figures that the vehicle moving at lower longitudinal velocity v_x renders more stability to the vehicle than compared to when the v_x is more.

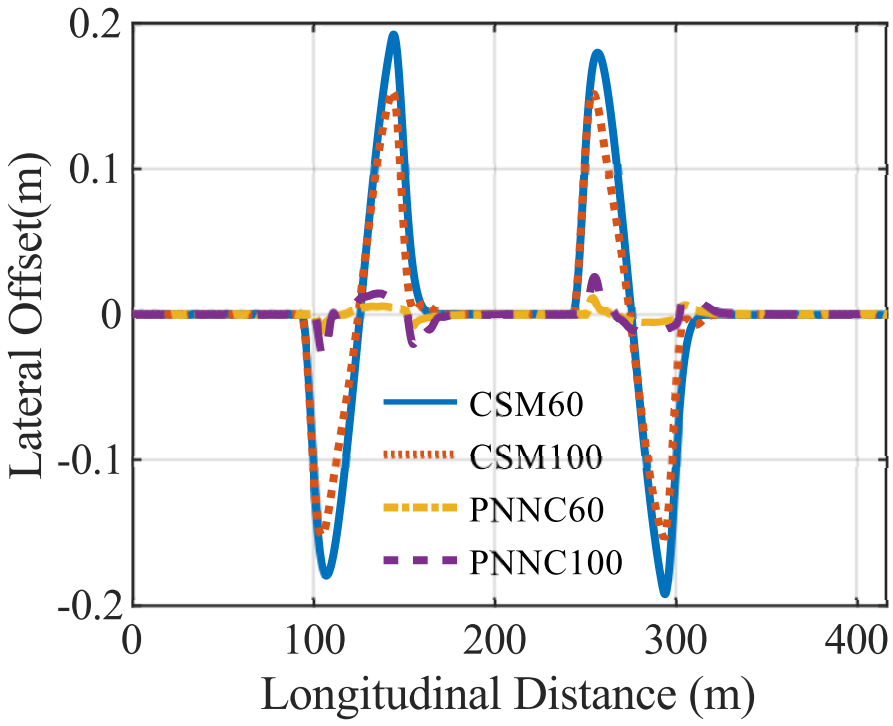

Figure 4. Lateral offset of the pure pursuit Model Predictive Control (MPC) controller and the proposed Neural Network controller (PNNC) for v_x = 60 km/h and v_x = 100 km/h.

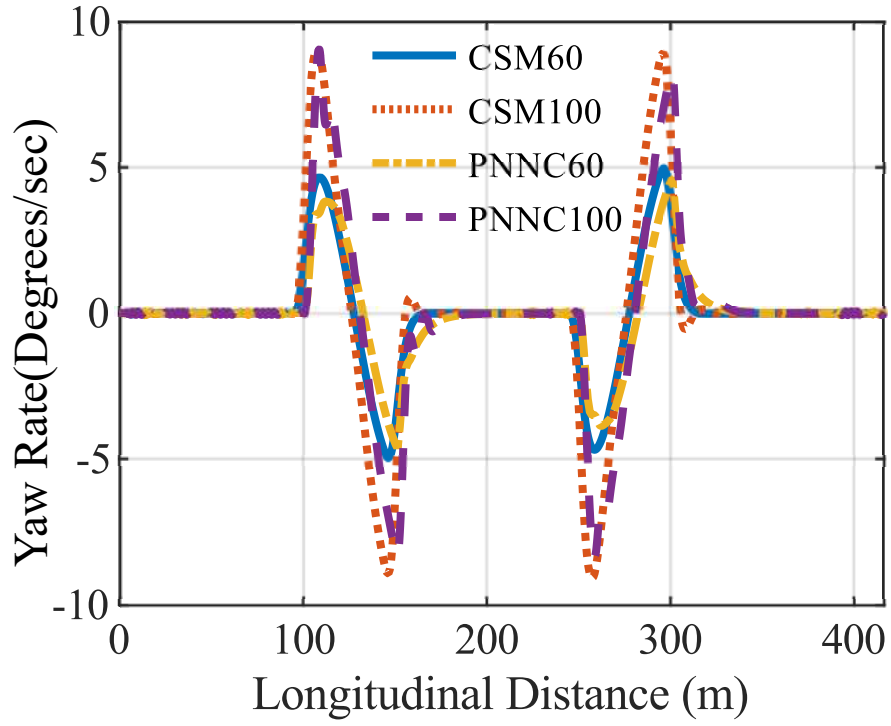

Figure 5. Yaw rate of the pure pursuit MPC controller (CSM) and the proposed Neural Network controller (PNNC) for v_x = 60 km/h and v_x = 100 km/h.

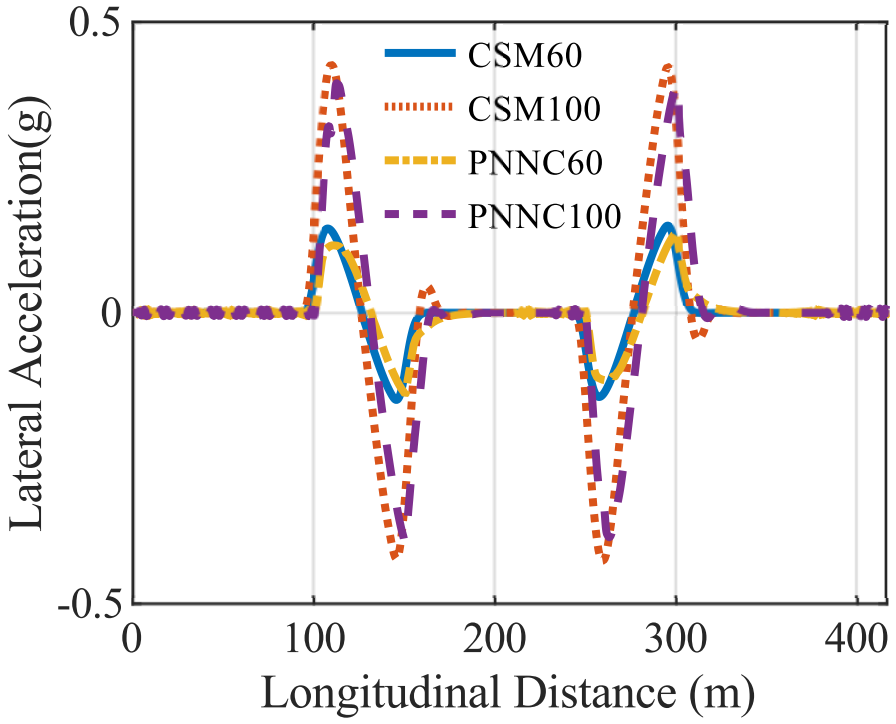

Figure 6. Lateral acceleration of the pure pursuit MPC controller and the proposed Neural Network controller (PNNC) for v_x = 60 km/h and v_x = 100 km/h.

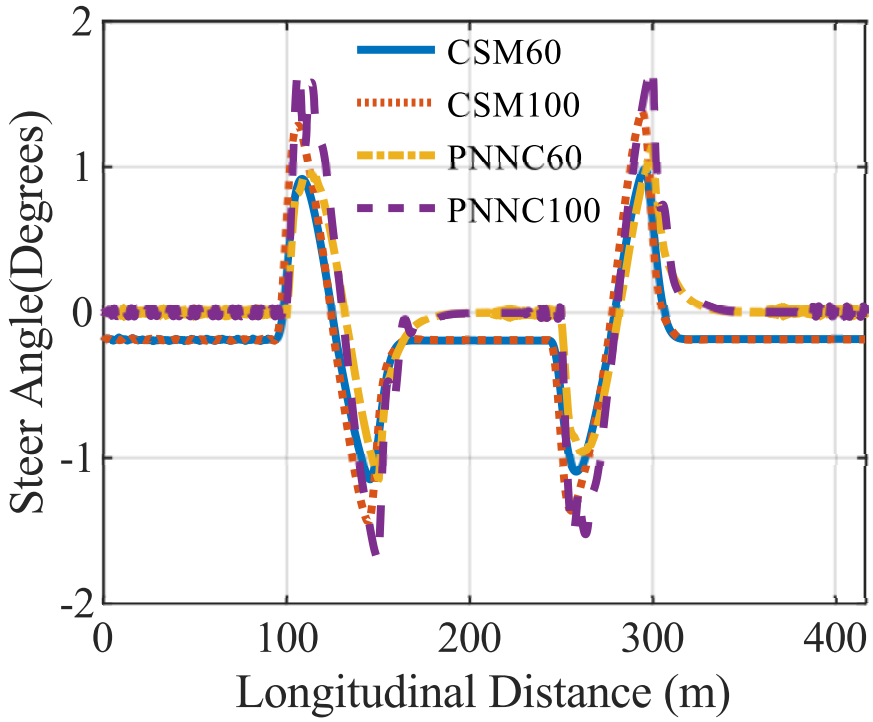

Figure 7. Road steer angle of the pure pursuit MPC controller and the proposed Neural Network controller (PNNC) for v_x = 60 km/h and v_x = 100 km/h.

5.2. Robustness to External Disturbances and a Variety of Road Conditions: $\mu \in$ [0.4–0.85] and $\mu = 1$, $v_x = 100$ km/h

In this first case, the vehicle is allowed to navigate on a road-surface where the friction μ varies between 0.4 to 0.85. In the second case, the vehicle is made to move on a road-surface where the road friction $\mu = 1$. In the third case, the performance of the vehicle when the road friction μ varies between 0.4 to 0.85 is simulated using the in-built MPC controller in CarSim. For all the cases, the vehicle moving at a high longitudinal speed v_x = 100 km/h is impacted with crosswinds as a disturbance between the longitudinal distance of 100 to 250 m. The performance of the RBFNN-HOSM controller in terms of lane-keeping and vehicle stability is examined under these adverse scenarios for the first two cases and is then compared with the in-built MPC controller in CarSim. Figure 8a,b shows the global reference path and the aerodynamics forces and the yaw-moment being impacted on the vehicle on its course. The global reference path resembles that of a double lane change trajectory. From Figure 8c,d, it is observed that the lateral offset and the heading error gets distorted when the vehicle is impacted with crosswinds at a longitudinal distance between 100 to 200 m when $\mu \in$ [0.4–0.85] for our proposed RBFNN-HOSM controller. However, after a distance of 200m, the effect of disturbances is compensated by the proposed RBFNN-HOSM controller. On the contrary, when $\mu = 1$ there is a slight deviation in the lateral offset and heading error at a longitudinal distance of 150 m but after the compensation provided by the proposed controller, the performance improves. The peak value of the lateral offset and the heading error is 0.1 m and 2 degrees, respectively, clearly signifying that the vehicle does not get deviated much even during the onset of adverse conditions. At a longitudinal distance of 250 m when there is a lane change in the global reference path, there is a little shift in the lateral offset and the heading error, which is again compensated thereafter. It is observed that the lateral offset and heading error in the case of the proposed RBFNN-HOSM controller is less than the in-built MPC controller in Carsim. The lateral acceleration and yaw-rate are more in the case of the in-built MPC controller in Carsim than compared to the proposed RBFNN-HOSM controller. Thus, from

Figure 8, it is observed that the performance of the proposed controller is better than the in-built MPC controller in Carsim.

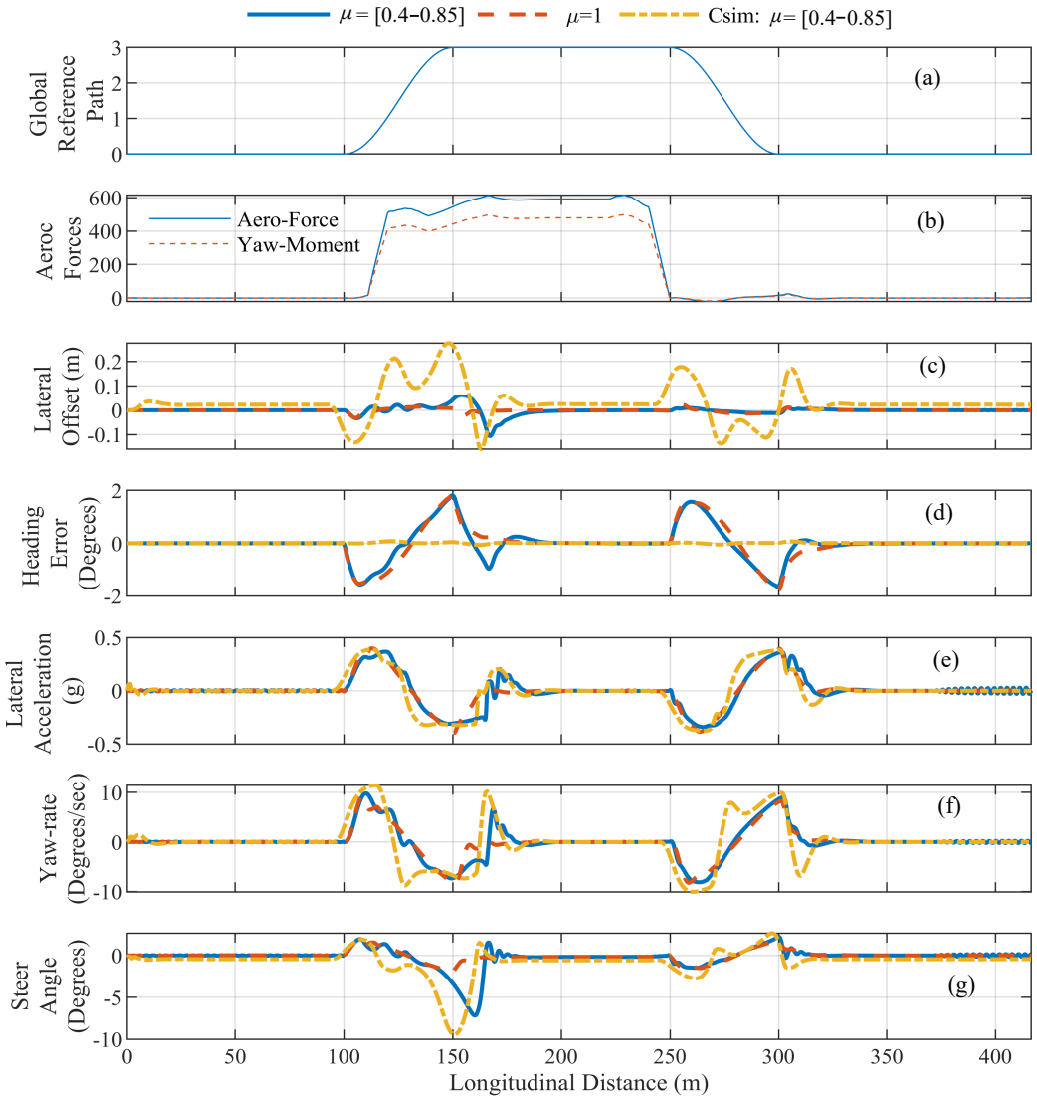

Figure 8. Lane keeping and vehicle stability performance of the proposed RBFNN-HOSM controller for v_x = 100 km/h in the presence of disturbances and a variety of road conditions and comparison with the in-built Carsim vehicle simulator, $\mu \in [0.4–0.85]$ and $\mu = 1$. (**a**) Global Reference Path, (**b**) Aero forces, (**c**) Lateral Offset, (**d**) Heading Error, (**e**) Lateral Acceleration, (**f**) Yaw Rate, (**g**) Road Steer Angle for various road conditions.

The peak value of the Lateral acceleration, as shown in Figure 8e, is 3.58 m/s^2, which states the fact that the vehicle operates in the region of the tire-road saturation limit. The deterioration in the lateral acceleration, during the case when $\mu \in [0.4–0.85]$, occurs due to the impact on the lateral force component at low friction conditions, as shown in Figure 9.

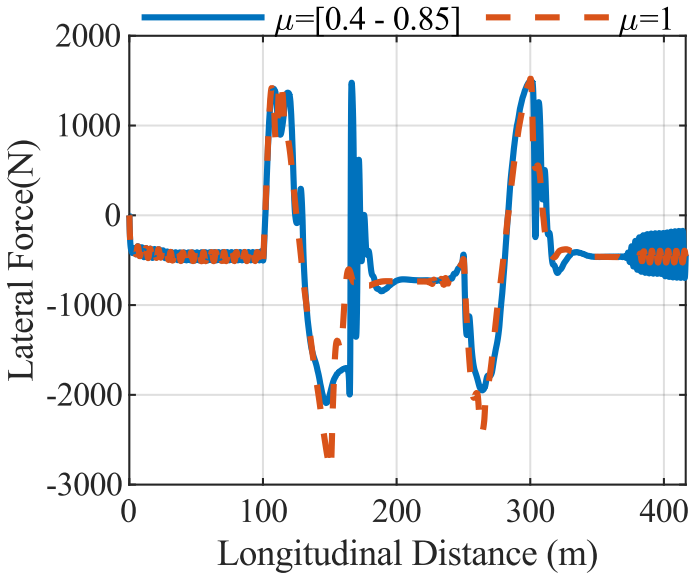

Figure 9. The behavior of lateral force for v_x = 100 km/h for a variety of road conditions, $\mu \in [0.4–0.85]$ and $\mu = 1$.

When $\mu \in [0.4–0.85]$, the yaw-rate shown in Figure 8f shows the sign of distortion during the time when the disturbance begins and reaches a peak value of 10 degrees/s in the case of our proposed RBFNN-HOSM controller. However, due to the compensation provided by the proposed controller, the distortion in the yaw-rate gets stabilized at a longitudinal distance of 200 m signifying the regaining of vehicle stability. The effect of disturbances and the road-surface friction is witnessed in the road steer angle when $\mu \in [0.4–0.85]$, as shown in Figure 8g, where there is a sharp increase in the steer angle during the time when the disturbance begins. On the contrary, when $\mu = 1$, there is a slight dip in the steering angle at the longitudinal distance of 150 m during the onset of crosswinds. However, the deviation in the steering angle when $\mu = 1$ gets compensated due to the control action provided by the proposed controller. The peak value of the steer angle rises to -6 degrees, but after the compensation provided by the proposed controller, the road steer angle exhibits smoothness and uniformity afterward. The effect on sliding surface due to the crosswinds and the different road conditions is shown in Figure 10. The effect of low-friction is clearly evident on the sliding surface characteristics with a sharp spike at a longitudinal distance of 150 m when $\mu \in [0.4–0.85]$.

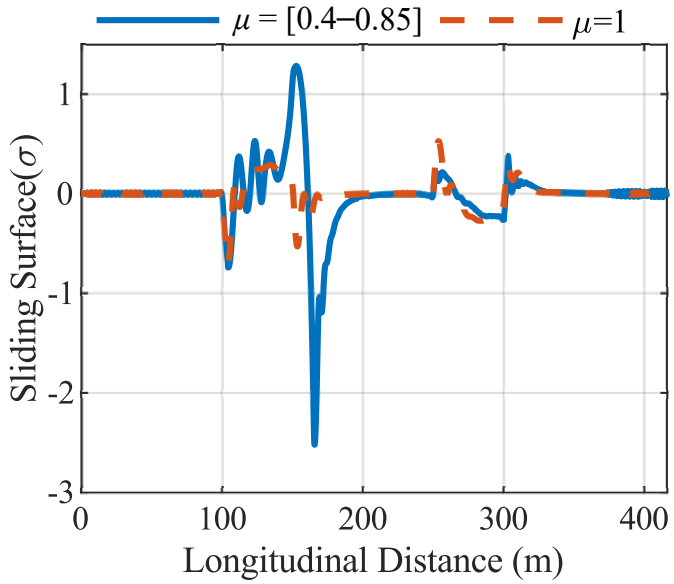

Figure 10. The effect on sliding surface for v_x = 100 km/h for a variety of road conditions, $\mu \in [0.4–0.85]$ and $\mu = 1$.

To further validate that the road-tire characteristics of the vehicle operate close to the region of saturation, the performance of lateral force on the vehicle is examined with respect to the tire-slip angle. In this study, the behavior of lateral force on the left front tire is examined with respect to the tire-slip angle. From Figure 11, it is observed that the road-tire characteristics exhibit the nonlinear behavior when the vehicle longitudinal speed is 100 km/h. In this case, the lateral force is saturated with the increase in the slip angle. However, at a lower longitudinal speed of 60 km/h, the tire road characteristics exhibit linear behavior, as shown in Figure 12.

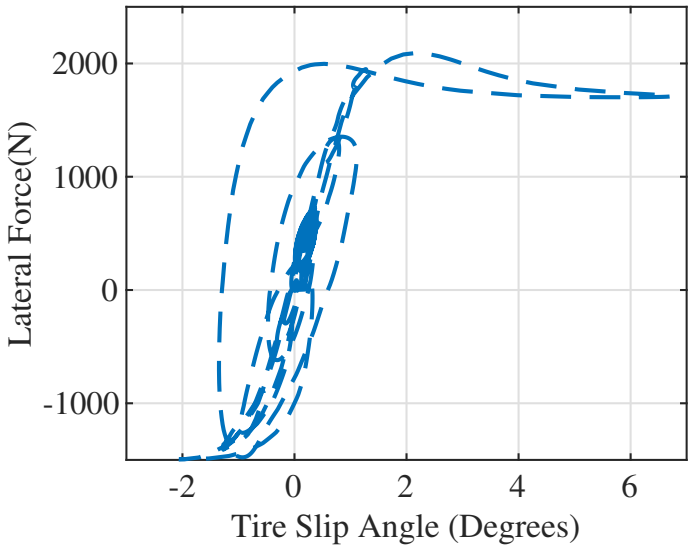

Figure 11. The behavior of lateral force with respect to the tire slip angle for v_x = 100 km/h in the presence of disturbance and a variety of road conditions, $\mu \in [0.4–0.85]$.

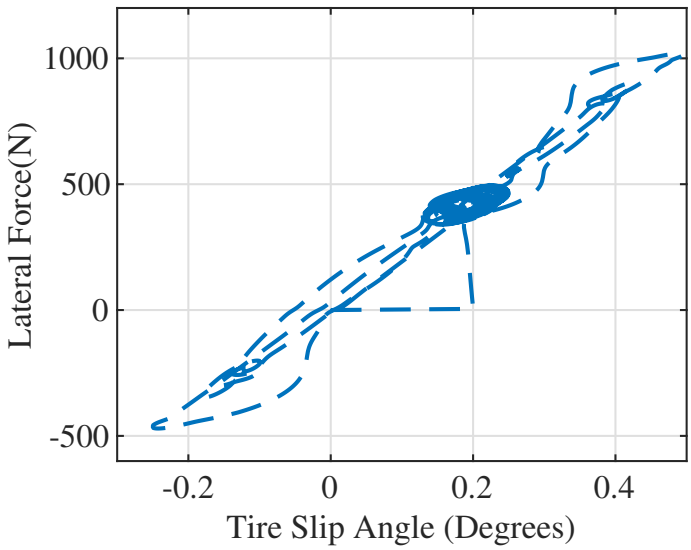

Figure 12. The behavior of lateral force with respect to the tire slip angle for v_x = 60 km/h in the presence of disturbance and a variety of road conditions, $\mu \in$ [0.2–0.85].

6. Discussion

The performance of the proposed controller is evaluated on the basis of the following categories

- **Lane keeping performance and lateral stability:** The ability of the proposed RBFNN-HOSM controller to ensure the lane-keeping performance and the stability under nominal conditions is shown in Figures 4–7. It is observed that the lateral offset and the heading error generated by the proposed controller are comparatively less than the inbuilt Carsim MPC pure-pursuit controller. The peak value of lateral acceleration for v_x = 60 km/h and v_x = 100 km/h for the proposed scheme is 7.15% and 30.87% less than the Carsim MPC pure-pursuit controller. However, one of the key components in the proposed controller performance is attributed to the judicious selection of cluster center and bias of the radial basis functions. It needs to be emphasized that an improper selection of cluster centers and bias will generate sub-optimal controller performance thereby degrading the lane-keeping performance.

- **Disturbance Rejection:** The ability of the proposed controller to compensate for the uncertainties and disturbances due to the effect of crosswinds is shown in Figure 8. The lane performance and the stability of the vehicle are affected in the presence of disturbances where the road friction coefficient μ varies between 0.4 and 1. However, due to the effect of the proposed RBFNN-HOSM controller the lane-keeping and the stability of the vehicle is again restored.
  - From Figure 12 in the presence of disturbances, it is observed that the vehicle moving at a lower longitudinal velocity v_x = 60 km/h exhibits linear tire-road characteristics. However, when the longitudinal velocity v_x = 100 km/h is increased, as shown in Figure 11, the tire-road characteristics approach the nonlinear region where the lateral force is saturated.
  - With the inclusion of the proposed controller, the disturbance rejection ability is achieved, as shown in Figures 8 and 13 at a longitudinal distance of 100–250 m.
  - Figures 8 and 13 show the performance of the vehicle in terms of lane-keeping and lateral stability for the longitudinal speed v_x = 100 km/h and v_x = 60 km/h in the presence of disturbances under a variety of road conditions. It is observed that for the vehicle moving at v_x = 100 km/h, the deviation in the lateral offset and heading error when $\mu = 1$ is comparatively much less than when $\mu \in$ [0.4–0.85].

- However, if we compare the performance of the lateral offset and the heading error for the above two longitudinal velocities, it is clearly evident that the vehicle moving at v_x = 60 km/h renders better lane-keeping control by generating comparatively less lateral offset and heading error as compared to v_x = 100 km/h.
- As far as lateral stability is concerned, the vehicle moving at v_x = 60 km/h renders more stability as the yaw-rate and the lateral acceleration has a smoother response with a very minimum deviation in the case of $\mu \in [0.2–0.85]$ compared to when $\mu = 1$. However, for the vehicle moving at v_x = 100 km/h the yaw-rate and the lateral acceleration shows signs of degradation in the case of low-friction $\mu \in [0.4–0.85]$ compared to when $\mu = 1$.

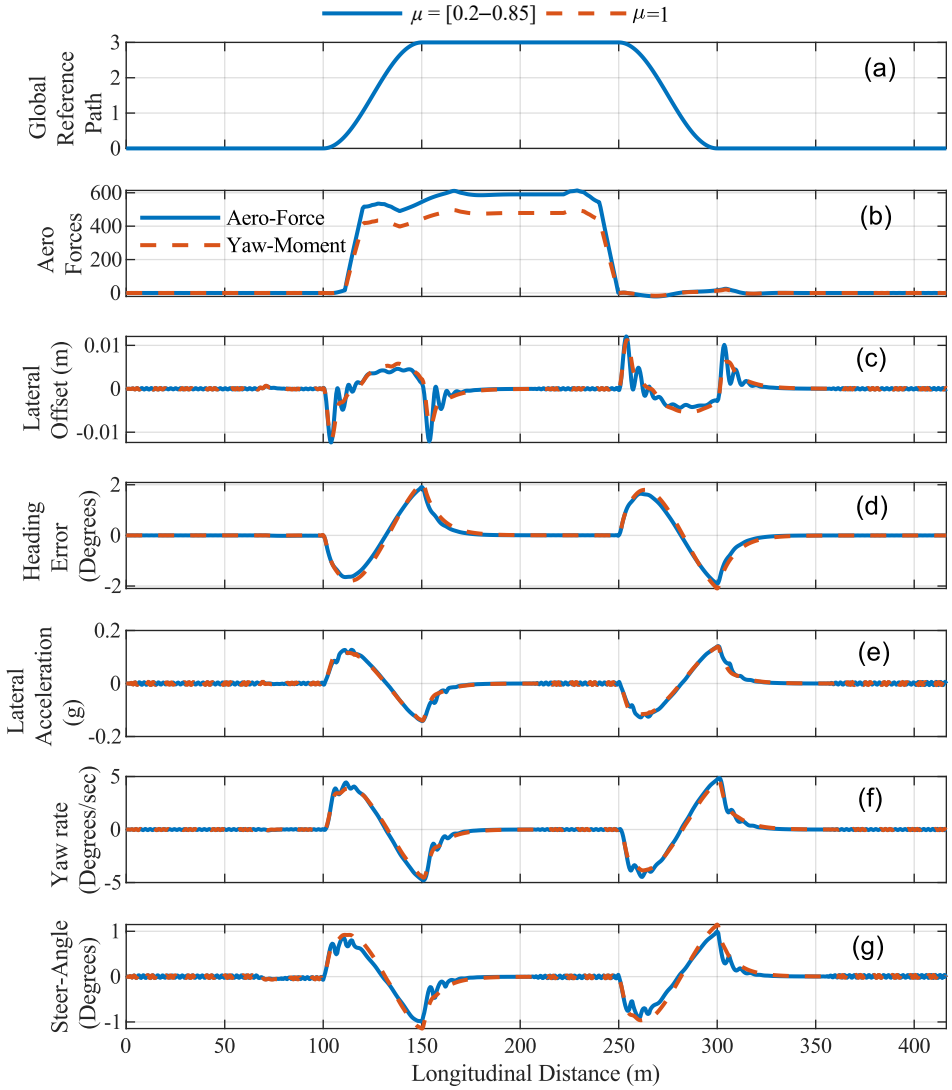

Figure 13. Lane keeping and vehicle stability performance of the proposed RBFNN-HOSM controller for v_x = 60 km/h in the presence of disturbances and a variety of road conditions, $\mu \in [0.2–0.85]$ and $\mu = 1$. (**a**) Global Reference Path, (**b**) Aero forces, (**c**) Lateral Offset, (**d**) Heading Error, (**e**) Lateral Acceleration, (**f**) Yaw Rate, (**g**) Road Steer Angle for various road conditions.

7. Conclusions

The present study is based on the estimation of the equivalent control by the proposed RBFNN on the account of unmeasured uncertainties and crosswinds as disturbances. The switching control or the discontinuous control is designed by the HOSM control. The combined effect of the equivalent and the switching control resulted in compensating

the effect of uncertainties and the disturbances on the lateral control and the stability of the vehicle. The increase in the longitudinal velocity of the vehicle in the presence of disturbances resulted in making the tire-road characteristics approach the nonlinear region. In the nominal scenario, it is observed that the lane-keeping performance and the lateral stability of the vehicle is enhanced by the use of the proposed controller compared to the inbuilt MPC based pure-pursuit controller in CarSim. During low-friction conditions in the presence of disturbances, the lateral stability and the lane offset errors were affected. However, the control action exhibited by the proposed controller ensured that the lane-keeping performance and the lateral stability of the vehicle is restored. In the future versions of the research work, the effect of longitudinal vehicle dynamics with other unmeasured suspension non-linearities will be integrated with the lateral dynamics to study the performance of the proposed RBFNN based HOSM controller on the overall lane-keeping and the lateral stability of the vehicle.

Author Contributions: The contributions made by the authors are as follows: S.K.S.; Overall Design Framework and methodology: S.K.S.; Simulation: S.K.S., J.J.R.; Result analysis and interpretation: S.K.S., J.J.R. and K.C.V.; Draft and Manuscript Preparation: K.C.V.; Overall supervision. All authors have read and agreed to the published version of the manuscript.

Funding: The research is supported by the National Research Foundation (NRF) of Korea through the Ministry of Education, Science and Technology under Grants NRF-2018R1A6A1A03025109.

Conflicts of Interest: The authors declare no conflict of interest.

References

1. Noy, I.Y.; Shinar, D.; Horrey, W.J. Automated driving: Safety blind spots. *Saf. Sci.* **2018**, *102*, 68–78. [CrossRef]
2. Brown, M.; Funke, J.; Erlien, S.; Gerdes, J.C. Safe driving envelopes for path tracking in autonomous vehicles. *Control Eng. Pract.* **2017**, *61*, 307–316. [CrossRef]
3. Lam, A.Y.S.; Leung, Y.; Chu, X. Autonomous-Vehicle Public Transportation System: Scheduling and Admission Control. *IEEE Trans. Intell. Transp. Syst.* **2016**, *17*, 1210–1226. [CrossRef]
4. Petrov, P.; Nashashibi, F. Modeling and Nonlinear Adaptive Control for Autonomous Vehicle Overtaking. *IEEE Trans. Intell. Transp. Syst.* **2014**, *15*, 1643–1656. [CrossRef]
5. Claussmann, L.; Revilloud, M.; Gruyer, D.; Glaser, S. A Review of Motion Planning for Highway Autonomous Driving. *IEEE Trans. Intell. Transp. Syst.* **2020**, *21*, 1826–1848. [CrossRef]
6. Guo, J.; Hu, P.; Li, L.; Wang, R. Design of Automatic Steering Controller for Trajectory Tracking of Unmanned Vehicles Using Genetic Algorithms. *IEEE Trans. Veh. Technol.* **2012**, *61*, 2913–2924. [CrossRef]
7. Liang, Y.; Li, Y.; Khajepour, A.; Ni, J.; Zheng, L. Holistic Adaptive Multi-Model Predictive Control for the path following of 4WID autonomous vehicles. *IEEE Trans. Veh. Technol.* **2020**, *70*, 69–81. [CrossRef]
8. Liang, Z.; Zhao, J.; Liu, B.; Wang, Y.; Ding, Z. Velocity-Based Path Following Control for Autonomous Vehicles to Avoid Exceeding Road Friction Limits Using Sliding Mode Method. *IEEE Trans. Intell. Transp. Syst.* **2020**, 1–12. [CrossRef]
9. Noh, S. Decision-Making Framework for Autonomous Driving at Road Intersections: Safeguarding Against Collision, Overly Conservative Behavior, and Violation Vehicles. *IEEE Trans. Ind. Electron.* **2019**, *66*, 3275–3286. [CrossRef]
10. Marino, R.; Scalzi, S.; Netto, M. Nested PID steering control for lane keeping in autonomous vehicles. *Control Eng. Pract.* **2011**, *19*, 1459–1467. [CrossRef]
11. Akermi, K.; Chouraqui, S.; Boudaa, B. Novel SMC control design for path following of autonomous vehicles with uncertainties and mismatched disturbances. *Int. J. Dyn. Control* **2020**, *8*, 254–268. [CrossRef]
12. Yuan, X.; Huang, G.; Shi, K. Improved Adaptive Path Following Control System for Autonomous Vehicle in Different Velocities. *IEEE Trans. Intell. Transp. Syst.* **2020**, *21*, 3247–3256. [CrossRef]
13. Matute-Peaspan, J.A.; Marcano, M.; Diaz, S.; Zubizarreta, A.; Perez, J. Lateral-Acceleration-Based Vehicle-Models-Blending for Automated Driving Controllers. *Electronics* **2020**, *9*, 1674. [CrossRef]
14. Farag, W. Complex Trajectory Tracking Using PID Control for Autonomous Driving. *Int. J. Intell. Transp. Syst. Res.* **2020**, *18*, 356–366. [CrossRef]
15. Guo, N.; Lenzo, B.; Zhang, X.; Zou, Y.; Zhai, R.; Zhang, T. A Real-Time Nonlinear Model Predictive Controller for Yaw Motion Optimization of Distributed Drive Electric Vehicles. *IEEE Trans. Veh. Technol.* **2020**, *69*, 4935–4946. [CrossRef]
16. Guo, N.; Zhang, X.; Zou, Y.; Lenzo, B.; Zhang, T. A Computationally Efficient Path-Following Control Strategy of Autonomous Electric Vehicles With Yaw Motion Stabilization. *IEEE Trans. Transp. Electrif.* **2020**, *6*, 728–739. [CrossRef]
17. Tork, N.; Amirkhani, A.; Shokouhi, S.B. An adaptive modified neural lateral-longitudinal control system for path following of autonomous vehicles. *Eng. Sci. Technol. Int. J.* **2021**, *24*, 126–137.

18. Nguyen, A.; Sentouh, C.; Zhang, H.; Popieul, J. Fuzzy Static Output Feedback Control for Path Following of Autonomous Vehicles With Transient Performance Improvements. *IEEE Trans. Intell. Transp. Syst.* **2020**, *21*, 3069–3079. [CrossRef]
19. Sarda, E.I.; Qu, H.; Bertaska, I.R.; von Ellenrieder, K.D. Station-keeping control of an unmanned surface vehicle exposed to current and wind disturbances. *Ocean Eng.* **2016**, *127*, 305–324. [CrossRef]
20. Wu, Y.; Wang, L.; Zhang, J.; Li, F. Path Following Control of Autonomous Ground Vehicle Based on Nonsingular Terminal Sliding Mode and Active Disturbance Rejection Control. *IEEE Trans. Veh. Technol.* **2019**, *68*, 6379–6390. [CrossRef]
21. Liu, J.; Gao, L.; Zhang, J.; Yan, F. Super-twisting algorithm second-order sliding mode control for collision avoidance system based on active front steering and direct yaw moment control. *Proc. Inst. Mech. Eng. Part D J. Automob. Eng.* **2021**, *235*, 43–54. [CrossRef]
22. Ji, X.; He, X.; Lv, C.; Liu, Y.; Wu, J. Adaptive-neural-network-based robust lateral motion control for autonomous vehicle at driving limits. *Control Eng. Pract.* **2018**, *76*, 41–53. [CrossRef]
23. Li, L.; Wang, H.; Lian, J.; Ding, X.; Cao, W. A Lateral Control Method of Intelligent Vehicle Based on Fuzzy Neural Network. *Adv. Mech. Eng.* **2015**. [CrossRef] [PubMed]
24. Hongbo, W.; Li, C.; Weihua, Z. Lane Keeping control based on an improved artificial potential method and coordination of steering/braking systems. *IET Intell. Transp. Syst.* **2019**, *13*, 1832–1842. [CrossRef]
25. Rath, J.J.; Senouth, C.; Popieul, J.C. Personalised lane keeping assist strategy: Adaptation to driving style. *IET Control Theory Appl.* **2019**, *13*, 106–115. [CrossRef]
26. Borroni, F.; Tanelli, M. A weighting approach to the shared-control of lateral vehicle dynamics. *IFAC-PapersOnLine* **2018**, *51*, 305–310. [CrossRef]
27. Rath, J.J.; Veluvolu, K.C.; Defoort, M.; Soh, Y.C. Higher-order sliding mode observer for estimation of tyre friction in ground vehicles. *IET Control Theory Appl.* **2014**, *8*, 399–408. [CrossRef]